Clinical Evaluation of Direct 4D Whole-Body PET Parametric Imaging with Time-of-Flight and Resolution Modeling Capabilities

Nicolas A. Karakatsanis[1], *Member, IEEE*, Abolfazl Mehranian[1], Martin A. Lodge[2], Michael E. Casey[3], Arman Rahmim[2,6], *Senior Member, IEEE* and Habib Zaidi[1,4,5], *Senior Member, IEEE*

***Abstract* – Whole-body (WB) PET parametric imaging has recently become clinically feasible with the introduction of multi-bed dynamic acquisition protocols, benefiting from the latest technologies in clinical PET scanners. Currently, Time-of-Flight (TOF) capabilities of modern PET systems allow for more accurate localization of the annihilation position along the line of response (LOR). As a result, TOF can prevent propagation, during image reconstruction, of various resolution degrading factors and noise beyond their origin and across the image space, thus providing i) an inherent correction or contrast recovery mechanism and ii) an effective sensitivity gain relative to non-TOF acquisitions. In addition, the incorporation of the PET system's point spread function (PSF) within the reconstruction system matrix has resulted in i) enhanced contrast and ii) considerably lower image roughness. Recently, we explored the effect of TOF and PSF on WB indirect Patlak imaging. In this work, we systematically investigate the additional benefit of TOF and PSF on clinical studies when reconstructing WB Patlak images directly from projection data. Therefore, we developed a nested direct 4D Patlak WB reconstruction algorithm capable of i) utilizing TOF information, ii) modeling PSF with an effective space-invariant Gaussian resolution kernel and iii) supporting both standard and generalized Patlak analysis. Our clinical evaluation on a set of WB dynamic clinical studies, as acquired with Siemens Biograph mCT TOF scanner, indicated a 15-30% target-to-background (TBR) and contrast-to-noise ratio (CNR) enhancement in all examined regions and for both Patlak methods, when only TOF feature is enabled, with an additional 5-10% improvement when combined with a 4mm FWHM Gaussian PSF kernel. Thus, we have demonstrated the benefits of integrating TOF and PSF features within a clinically adoptable direct 4D WB generalized Patlak reconstruction scheme.**

I. Introduction

DYNAMIC PET imaging has recently been extended from single bed to whole-body (WB) field-of-views (FOVs) by exploiting novel multi-bed PET data acquisition protocols, optimized for fast clinical adoption and supporting easily applicable and robust post-reconstruction, also known as indirect, parameter estimation methods of enhanced quantitative performance [1,2]. In addition, clinical feasibility of WB parametric PET imaging has been further improved nowadays, thanks to i) the overall higher sensitivity of modern clinical PET scanners, currently allowing for faster data acquisitions while retaining the same count statistics as previously [3-5], and ii) the development of highly efficient direct spatiotemporal (4-dimensional, 4D) parametric image reconstruction algorithms, limiting noise propagation in the final parametric images [6,7]. Moreover, a key point is iii) the incorporation within 4D reconstruction of robust Patlak graphical analysis which only requires tracking of intermediate or late (>10min post injection) tracer kinetics, thus alleviating the need for fast temporal WB sampling at early times [1,8].

Nevertheless, WB parametric PET imaging could also considerably benefit by two important state-of-the-art PET technological developments: i) the Time-of-Flight (TOF) PET acquisitions [9] and ii) Point Spread Function (PSF) image reconstruction methods [10]. Although they have only recently been introduced in commercial clinical PET scanners, TOF and PSF features have already been routinely applied in the clinic, delivering improved image quality with promising future prospects [11-20].

In particular, the capability of acquiring TOF information on modern clinical PET systems have already been associated with a significant improvement in contrast recovery and image resolution, especially for regions of low or moderate activity uptake [3]. At the same time, the current precision of TOF measurements, as determined by the current commercial PET scanner performance metric of TOF timing resolution, is still moderate with large margins of improvement to cover in future. The current trend indicates significant TOF resolution enhancements for the next generations of PET scanners, thus feeding reasonable expectations for further TOF-related benefits in the following years [21-24]. Dynamic PET imaging and especially its WB extension, could particularly exploit these benefits to significantly enhance image quality of short dynamic PET frames [25-28], or alternatively improve time sampling across multi-bed FOVs [1,29,30]. In addition, direct 4D parametric image reconstruction could also utilize TOF information to further enhance contrast and limit noise as well as kinetic-induced error propagation within and between correlated parametric images [31].

This work was supported by the Swiss National Science Foundation under Grant SNSF 31003A-149957 and by Siemens Medical Solutions.

[1] N. A. Karakatsanis (e-mail: nikolaos.karakatsanis@unige.ch) and H. Zaidi are with the Division of Nuclear Medicine and Molecular Imaging, School of Medicine, University of Geneva, Geneva, Switzerland

[2] M. A. Lodge and A. Rahmim are with the Department of Radiology, School of Medicine, Johns Hopkins University, Baltimore, MD, USA

[3] M. E. Casey is with Siemens Medical Solutions, Knoxville, TN, USA

[4] H. Zaidi is also with Geneva Neuroscience Centre, University of Geneva, Geneva, Switzerland

[5] H. Zaidi is also with the Department of Nuclear Medicine and Molecular Imaging, University of Groningen, Groningen, Netherlands

[6] A. Rahmim is also with the Department of Electrical & Computer Engineering, Johns Hopkins University, Baltimore, MD, USA.

978-1-4673-9862-6/15/$31.00 ©2015 IEEE

Furthermore, the employment of PSF resolution modeling within tomographic image reconstruction, as currently supported by clinical reconstruction software, has shown its clinical potential in effectively reducing partial volume effect (PVE) and enhancing contrast-to-noise ratio (CNR) scores especially in small regions of higher or low uptake than their surroundings [10,14,16-20]. PSF model-based reconstruction schemes can outperform image-based post-filtering methods by more accurately characterizing the resolution response of a PET system during the image generation process rather than afterwards [29,32]. Moreover, direct 4D parametric reconstruction [6,42] could particularly benefit by integrating PSF resolution modeling within its framework, as critical regions for the image-based extraction of the input function, such as the heart ventricles, and important target regions, such as tumors, can be susceptible to PVE-induced bias which, in turn, could be further propagated through 4D reconstruction [31,33-41].

Recently, we explored the effect of TOF and PSF technologies on WB indirect Patlak imaging, i.e. when voxel-wise post-reconstruction Patlak analysis is conducted [29]. However, in a parallel study we observed the importance of direct 4D WB Patlak imaging in reducing the high noise levels and increasing the low CNR scores of indirect Patlak images [6,42]. Therefore, in this work we systematically investigate on patient studies the additional benefit of TOF and PSF features, when integrated within 4D Patlak WB reconstruction. Our aim is the optimization of the presented 4D WB PET TOF+PSF reconstruction methods for routine clinical application, especially when combined with synthesized SUV imaging in the context of our recently proposed combined SUV/Patlak imaging framework [43].

II. Methods and Materials

A. Time-of-Flight PET Acquisition

The ability of modern fast PET detector systems to estimate, within a certain precision, the detection times of the two emitted gamma photons participating in each coincidence event enables calculation of their time-of-flight between annihilation and detection points and thus of their approximate annihilation position along the line-of-response (LOR) connecting the two detection points [9,44-49]. The TOF resolution of the system determines the precision of the estimated annihilation point and thus the minimum length of TOF segments to reliably collimate the counts along each LOR [50,51]. Unlike conventional non-TOF reconstruction which considers a uniform counts distribution along the entire LOR, advanced TOF reconstruction can utilize TOF-based LOR partitioning to more accurately model the counts distribution along the LOR and, as a result, enhance accuracy and precision in the reconstructed images [28,52]. Therefore, utilization of TOF information can effectively prevent during image reconstruction the propagation of noise as well as of various data inconsistencies, such as in attenuation, normalization and scatter correction, beyond their origin and across the image space, thus providing i) an inherent correction or contrast recovery mechanism and ii) an effective sensitivity gain relative to non-TOF acquisitions [9,29,53,54].

B. Point Spread Function Resolution Modeling

The integration of the PET system's resolution response, as characterized by its 3-dimensional (3D) point spread function (PSF), within the forward- and back-projection operators of a tomographic image reconstruction algorithm, commonly referred to as PSF reconstruction or resolution modeling [18,19,20,32-34,55], has recently been introduced in the software of commercial clinical PET systems [4,10,56]. PSF resolution modeling, when incorporated into the system matrix, can effectively trigger an iterative deconvolution of the modeled finite PSF resolution response from the reconstructed image and effectively improve the resulting images resolution at the boundaries between two regions of different activity levels while reducing image roughness in uniform regions [32]. In this study, we have utilized so far a 3D space invariant Gaussian PSF kernel which could be a simple, effective and readily adopted resolution modeling tool for a range of clinical PET scanners. However, PSF deconvolution also tends to enhance inter-voxel correlations resulting in so-called Gibbs artifacts which may affect reproducibility and quantification, two critical features in parametric PET imaging [10,32,56-59]. Therefore, we utilized a PSF kernel of slightly smaller 3D Gaussian FWHM size than the reported spatial resolution of our PET scanner, motivated by recent studies which have demonstrated reduction of Gibbs artifacts when partial PSF resolution modeling is applied [60,61].

C. Direct 4D TOF+PSF WB Patlak Image Reconstruction

In this work, we investigate the additional benefit of TOF and PSF features when reconstructing WB Patlak images directly from projection data [6,7,62-65]. For that purpose we utilized a direct 4D Patlak WB reconstruction algorithm, supporting both standard (sPatlak) [8] and generalized Patlak (gPatlak) analysis [66-69] and employing the concept of optimization transfer for accelerated convergence [42,66,70,71]. Previously, the algorithm has been developed and evaluated for non-TOF simulated data [42].

Currently, we added the capabilities of i) TOF information utilization and ii) PSF resolution modeling within the tomographic reconstruction system matrix and conducted a systematic patient evaluation study. Furthermore, to avoid trapping to local optima and ensure proper convergence for the non-linear gPatlak algorithm, sPatlak reconstructed images after 3 full OS-EM iterations (21 subsets) have been used to initialize gPatlak reconstruction for subsequent iterations.

D. Design of clinical evaluation study

Our clinical evaluation was performed on a set of WB dynamic PET FDG clinical studies acquired on state-of-the-art Siemens Biograph mCT TOF PET/CT scanner with reported TOF resolution of 580ps FWHM and a measured PSF of 4.1mm FWHM at the FOV center [4]. For partial PSF

resolution recovery, we applied a slightly smaller Gaussian kernel of 4.0mm FWHM within the 4D reconstruction [60,61].

The clinical studies have been acquired over a 60-78min post injection window [43], which is similar with the standard scan window of conventional standard-of-care static SUV WB PET scans to facilitate its clinical feasibility and adoption. Since the initial 1h post-injection data of the input function cannot be acquired with such a protocol, the missing section of the individual patients input functions have been derived by properly scaling a previously calculated population-based complete input function from a set of 11 patient studies [72,73]. The scaling has been applied such that the late measurements of each individual input function matched on average the corresponding late section of the population-based model. The modeled input function had been initially cross-validated with the leave-one-out method [73].

The protocol has been streamlined for clinical feasibility and, thus involved 4 WB unidirectional (cranio-caudal) passes, each equal in time duration and consisting of 6 beds with constant bed frames of 45sec, as previously optimized for non-TOF case [1]. For comparative evaluation purposes, the non-TOF raw clinical data have been produced from the corresponding TOF data after summing up all 13 TOF bins of the mCT raw projection data. In future, we are planning to also evaluate shorter bed frames, i.e. of 30sec duration, to allow for 6 WB passes within the same total scan time window and, thus exploit the effective PET sensitivity gain of 580ps TOF resolution compared to non-TOF acquisitions [4,10].

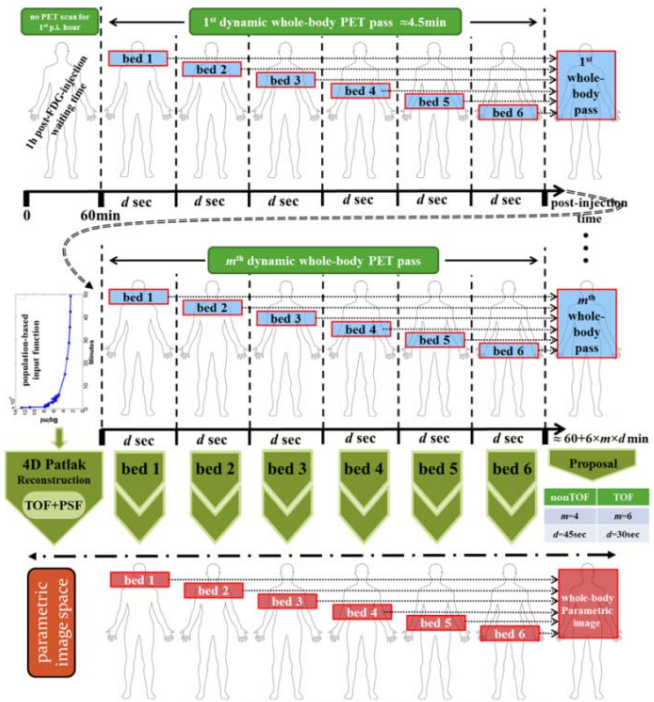

Fig. 1: (First 2 rows): WB dynamic acquisition, involving m WB passes, each consisting of equal bed frames of d sec. The recommended values for the m and d parameters are provided for both non-TOF and TOF cases at the table located at the bottom right of the figure. (Bottom row): Production of 4D (s/g)Patlak TOF+PSF WB images using a previously proposed population-based input function method, after validating it with a leave-one-out cross-validation method on a set of eleven patient studies, all acquired at Johns Hopkins PET center [73].

The single-frame, i.e. static, WB SUV images for each patient have been synthesized after adding all decay-corrected raw projection data acquired frames at each bed position. The resulting sinograms can then be reconstructed with proper normalization to generate the equivalent SUV image. Alternatively, the SUV image could be estimated with a more straightforward post-reconstruction method. In particular, all individual data frames of each bed could first be reconstructed independently using the commercial scanner software, followed by simple summation of the resulting dynamic image frames at each bed position. The final WB image can then be easily constructed from the individual bed position images. Our preliminary clinical evaluation study on a pilot set of 5 patients has found negligible differences between the two methods for the level of count statistics observed with our proposed protocol on the TOF Biograph mCT clinical scanner [1,4,73].

III. Results and Discussion

Our quantitative evaluation was conducted on a set of liver and thorax regions, as drawn from synthesized SUV clinical PET images after adding all 4 WB passes at the projection data level and then reconstructing (Fig. 2) [43]. The count statistics are equivalent to 3min per bed (addition of 4 frames, each of 45sec) and thus may be considered sufficient for a satisfactory accuracy in the ROIs delineation, as illustrated in Fig. 2.

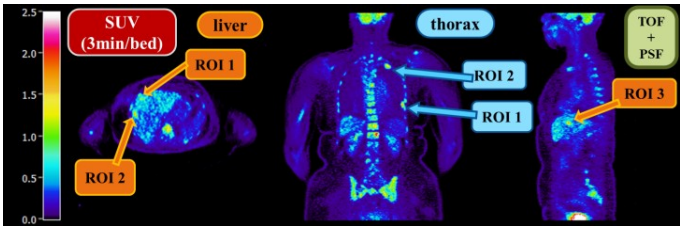

Fig. 2. Regions in the liver and thorax evaluated in this study, as drawn from synthesized SUV images after adding all 4 WB passes data acquired between 60-78min [7].

The WB parametric images of tracer influx rate constant K_i , also known as Patlak slope, in Fig. 3 indicate a 15-30% target-to-background (TBR) and CNR enhancement in all evaluated regions and for both Patlak graphical analysis methods, compared to non-TOF and non-PSF case, when only TOF feature is enabled. An additional 5-10% improvement was observed, relative to the same class of data, when TOF feature was combined with PSF reconstruction (TOF+PSF). It should also be noted that PSF feature alone did reduce noise for the same attained contrast levels, regardless of the availability of TOF information.

Our results reproduce the same performance trend as previously observed on static PET data [12,14,74], as well as post-reconstruction Patlak K_i analysis [29]. Moreover, TOF+PSF Patlak K_i images consistently demonstrated higher lesion TBR contrast and CNR scores than that of TOF+PSF SUV images, thus confirming previous findings for non-TOF

+ non-PSF comparisons between K_i and SUV PET images [1,2,65]. This observation suggests the additional benefit of enriching established SUV imaging with complementary parametric information through combined SUV/Patlak clinically adoptable imaging protocols [43].

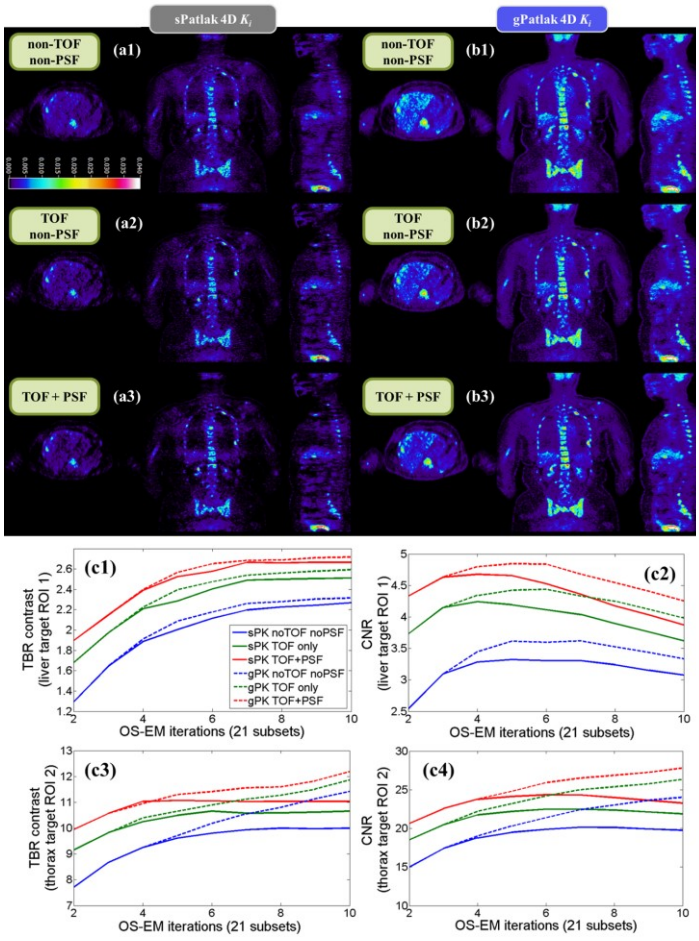

Fig. 3. K_i sPatlak (a1-a3) and gPatlak (b1-b3) patient WB images employing various combinations of TOF and PSF features. TBR and CNR plots for target K_i ROIs in liver (c1, c2) and thorax (c3, c4). Both 4D (s/g)Patlak methods (sPK & gPK) are evaluated. The direct 4D gPatlak (gPK) reconstruction algorithm has been initialized with the respective sPatlak (sPK) image estimates of the 3rd OS-EM iteration, thus the results are identical for the first 3 OS-EM iterations.

Furthermore, in Fig. 4 TOF+PSF direct 4D Patlak reconstruction achieved higher TBR and CNR scores in the evaluated lesion ROIs than TOF + post-reconstruction smoothing for the same space-invariant FWHM Gaussian kernel size. This observation suggests that PSF reconstruction alone does improve the trade-off between resolution and noise in the Patlak K_i images and therefore its preference over simple post-smoothing can be justified for direct 4D WB Patlak K_i imaging, in addition to previous similar findings for indirect K_i [29] as well as static SUV PET images [16-20].

Finally, the generalized 4D Patlak (gPK) TBR and CNR curves were systematically converging to a relatively higher score than respective standard 4D Patlak (sPK) curves in both fig. 3 and 4, thus reproducing the same performance trend with our previous findings for indirect application of the respective WB Patlak analysis methods [64,65]. We attribute the superior TBR and CNR performance of gPatlak to its ability to better account for potential tracer uptake reversibility with respect to standard linear Patlak model [8].

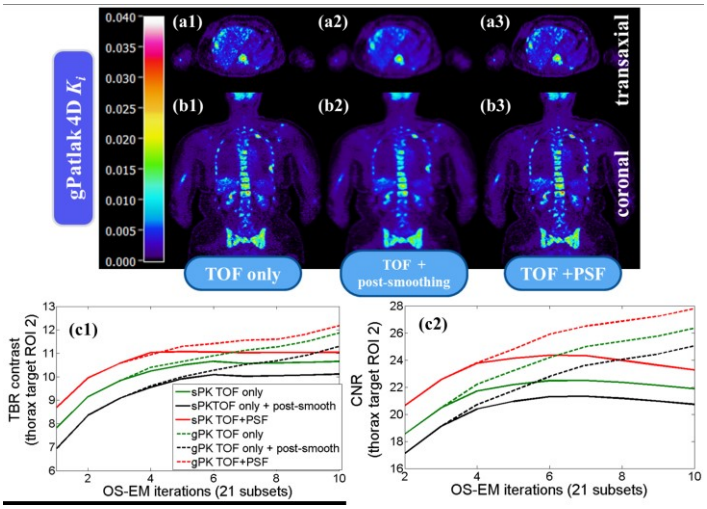

Fig. 4. Transaxial (a1-a3) and coronal (b1-b3) K_i images for TOF w. & w/o PSF modeling as well as TOF+post-smoothing. Respective TBR (c1) and CNR (c2) plots for a target K_i ROI in thorax. Both 4D (s/g)Patlak methods are evaluated. The direct 4D gPatlak (gPK) reconstruction algorithm has been initialized with the respective sPatlak (sPK) image estimates of the 3rd OS-EM iteration, thus the results are identical for the first 3 OS-EM iterations.

We should note here that gPatlak 4D reconstruction was initialized for the first 3 OS-EM iterations with linear sPatlak reconstruction estimates to ensure global optimal EM convergence by avoiding the possibility of trapping to any local optima, due to the non-linearity of the gPatlak objective function [42]. Since our proposed SUV/Patlak combined imaging protocol is restricted to late time-windows for clinical adoptability, the potential bias in the Patlak K_i estimates, due to lack of early tracer kinetics data [75], may be sufficiently compensated through a robust 4D reconstruction of gPatlak analysis, further supported by TOF+PSF features utilization.

IV. Conclusions

Our patient results consistently demonstrated the additional clinical benefits in TBR and CNR performance when direct 4D WB (s/g)Patlak reconstruction utilizes the current TOF and PSF reconstruction capabilities of modern commercial PET/CT scanners to further enhance lesion detectability and quantification imaging tasks. In addition, we have shown the clinical feasibility of direct 4D WB Patlak imaging as well as it clinical potential when combined, as a complementary feature, with routinely established SUV imaging within a unified SUV/Patlak WB imaging framework. Finally, we note the superior TBR and CNR performance of gPatlak analysis on clinical data, when supported by efficient 4D reconstruction as well as TOF+PSF features to limit noise and error propagation in the final image estimates.

V. ACKNOWLEDGMENTS

The authors would like to gratefully acknowledge support by Siemens Medical Solutions and the Swiss National Science Foundation under Grant SNSF 31003A-149957.

REFERENCES

[1] N. A. Karakatsanis, M. A. Lodge, A. K. Tahari, Y. Zhou, R. L. Wahl and A. Rahmim, "Dynamic whole-body PET parametric imaging: I. Concept, acquisition protocol optimization and clinical application," Phys. Med. Biol., 58(20), p. 7391-7418, 2013

[2] N. A. Karakatsanis, M. A. Lodge, Y. Zhou, R. L. Wahl and A. Rahmim, "Dynamic whole-body PET parametric imaging: II. Task-oriented statistical estimation," Phys. Med. Biol., 58(20), p. 7419-7445, 2013

[3] R. Boellaard, A. van Lingen, and A. A. Lammertsma, "Experimental and clinical evaluation of iterative reconstruction (OSEM) in dynamic PET: quantitative characteristics and effects on kinetic modeling," J Nucl Med, 42(5), p. 808-817, 2001

[4] B. W. Jakoby, Y. Bercier, M. Conti, M. E. Casey, B. Bendriem and D. W. Townsend, "Physical and clinical performance of the mCT time-of-flight PET/CT scanner," Phys Med Biol, 56(8), p. 2375-2389, 2011

[5] V. Y. Panin, A M Smith, J Hu, F. Kehren and M. E. Casey, "Continuous bed motion on clinical scanner: design, data correction, and reconstruction," Phys Med Biol, 59(20), p. 6153-6174, 2014

[6] N. A. Karakatsanis, M. A. Lodge, R. L. Wahl and A. Rahmim, "Direct 4D whole-body PET/CT parametric image reconstruction: concept and comparison vs. indirect parametric imaging," J Nucl Med, 54 (Supplement 2), p. 2133-2133, 2013

[7] W. Zhu, Q. Li, and R. M. Leahy, "Dual-time-point Patlak estimation from list mode PET data," IEEE Int Symp Biom Imag (ISBI), p. 486-489, 2012

[8] C. S. Patlak, R. G. Blasberg, and J. D. Fenstermacher, "Graphical evaluation of blood-to-brain transfer constants from multiple-time uptake data," J. Cereb. Blood Flow Metab., 3(1), p. 1-7, 1983

[9] J. S. Karp, S. Surti, M. E. Daube-Witherspoon and G. Muehllehner, "Benefit of time-of-flight in PET: experimental and clinical results," J Nucl Med, 49(3), p. 462-470, 2008

[10] V. Y. Panin, F. Kehren, C. Michel and M. Casey, "Fully 3-D PET reconstruction with system matrix derived from point source measurements, IEEE Trans Med Imag, 25(7), p. 907-921, 2006

[11] S. Surti, and J. S. Karp, "Experimental evaluation of a simple lesion detection task with time-of-flight PET," Phys Med Biol, 54(2), p. 373-384, 2009

[12] D. J. Kadrmas, M. E. Casey, M. Conti, B. W. Jakoby, C. Lois, and D. W. Townsend, "Impact of time-of-flight on PET tumor detection," J Nucl Med, 50(8), p. 1315-1323, 2009

[13] C. Lois, B. W. Jakoby, M. J. Long, K. F. Hubner, D. W. Barker, M. E. Casey, M. Conti, V. Y. Panin, D. J. Kadrmas, and D. W. Townsend, "An assessment of the impact of incorporating time-of-flight information into clinical PET/CT imaging," J Nucl Med, 51(2), p. 237-245, 2010

[14] J. Schaefferkoetter, M. Casey, D. Townsend, and G. El Fakhri, "Clinical impact of time-of-flight and point response modeling in PET reconstructions: a lesion detection study," Phys Med Biol, 58(5), p. 1465-1478, 2013

[15] S. Surti, "Update on time-of-flight PET imaging," J Nucl Med, 56(1), p. 98-105, 2015

[16] F. C. Sureau, A. J. Reader, C. Comtat, C. Leroy, M. J. Ribeiro, I. Buvat, and R. Trébossen, "Impact of image-space resolution modeling for studies with the high-resolution research tomograph," J Nucl Med, 49(6), p. 1000-1008, 2008

[17] A. Varrone, N. Sjöholm, L. Eriksson, B. Gulyás, C. Halldin, and L. Farde, L, "Advancement in PET quantification using 3D-OP-OSEM point spread function reconstruction with the HRRT," Eur J Nucl Med Mol Imag, 36(10), p. 1639-1650, 2009

[18] A. M. Alessio, C. W. Stearns, S. Tong, S. G. Ross, S. Kohlmyer, A. Ganin, and P. E. Kinahan, "Application and evaluation of a measured spatially variant system model for PET image reconstruction, " IEEE Trans Med Imag, 29(3) p. 938-949, 2010

[19] S. Tong, A. M. Alessio, and P. E. Kinahan, "Noise and signal properties in PSF-based fully 3D PET image reconstruction: an experimental evaluation," Phys Med Biol, 55(5), p. 1453-1473, 2010

[20] E. Rapisarda, V. Bettinardi, K. Thielemans, and M. C. Gilardi, "Image-based point spread function implementation in a fully 3D OSEM reconstruction algorithm for PET," Phys Med Biol, 55(14), p. 4131-4151, 2010

[21] W. W. Moses, and S. E. Derenzo, S. E. "Prospects for time-of-flight PET using LSO scintillator," IEEE Trans Nucl Sc, 46(3), p. 474-478, 1999

[22] D. R. Schaart, S. Seifert, R. Vinke, H. T. van Dam, P. Dendooven, H. Löhner, and F. J. Beekman, "LaBr3: Ce and SiPMs for time-of-flight PET: achieving 100 ps coincidence resolving time," Phys Med Biol, 55(7), p. N179-N189, 2010

[23] S. Seifert, H. T. van Dam, J. Huizenga, R. Vinke, P. Dendooven, H. Löhner and D. R. Schaart, D. R., "Monolithic LaBr3: Ce crystals on silicon photomultiplier arrays for time-of-flight positron emission tomography," Phys Med Biol, 57(8), p. 2219-2233, 2012

[24] H. T. Van Dam, G. Borghi, S. Seifert, and D. R. Schaart, "Sub-200 ps CRT in monolithic scintillator PET detectors using digital SiPM arrays and maximum likelihood interaction time estimation," Phys Med Biol, 58(10), p. 3243-3257, 2013

[25] M. M. Ter-Pogossian, and M. Michel, "Special characteristics and potential for dynamic function studies with PET," Sem Nucl Med, 11(1), p. 13-23, 1981

[26] N. A. Mullani, J. Gaeta, K. Yerian, W-H. Wong, R. K. Hartz, E. A. Philippe, D. Bristow, and K. L. Gould, "Dynamic imaging with high resolution time-of-flight PET camera-TOFPET I," IEEE Trans Nucl Sci, 31(1), p. 609-613, 1984

[27] W. Wang, Z. Hu, E. E. Gualtieri, M. J. Parma, E. S. Walsh, D. Sebok, Y. L. Hsieh, C. H. Tung, X. Song, J. J. Griesmer, J. A. Kolthammer, L. M. Popescu, M. Werner, J. S. Karp and D. Gagnon, "Systematic and distributed time-of-flight list mode PET reconstruction," IEEE Nucl Sc Symp Med Imag Conf (NSS/MIC), p. 1715-1722, 2006

[28] M. Conti, "State of the art and challenges of time-of-flight PET," Physica Medica, 25(1), p. 1-11, 2009

[29] N. A. Karakatsanis, M. A. Lodge, A. Rahmim, and H. Zaidi, "Introducing Time-of-Flight and Resolution Recovery Image Reconstruction to Clinical Whole-body PET Parametric Imaging," IEEE Nucl Sc Symp Med Imag Conf (NSS/MIC), 2014

[30] F. A. Kotasidis, C. Tsoumpas, and A. Rahmim, "Advanced kinetic modelling strategies: towards adoption in clinical PET imaging," Clin Trans Imag, 2(3), p. 219-237, 2014

[31] F. Kotasidis, J. C. Matthews, G. Angelis, P. J. Markiewicz, W. R. Lionheart and A. J. Reader, "Impact of erroneous kinetic model formulation in Direct 4D image reconstruction," IEEE Nucl Sc Symp Med Imag Conf (NSS/MIC), p. 2366-2367, 2011

[32] A. Rahmim, J. Qi, and V. Sossi, "Resolution modeling in PET imaging: theory, practice, benefits, and pitfalls," Med Phys, 40(6), 064301, 2013

[33] G. Brix, J. Doll, M. E. Bellemann, H. Trojan, U. Haberkorn, P. Schmidlin, and H. Ostertag, H, "Use of scanner characteristics in iterative image reconstruction for high-resolution positron emission tomography studies of small animals," Eur J Nucl Med Mol Imag, 24(7), p. 779-786, 1997

[34] A. J. Reader, P. J. Julyan, H. Williams, D. L. Hastings, and J. Zweit, J. "EM algorithm system modeling by image-space techniques for PET reconstruction," IEEE Trans Nucl Sc, 50(5), p. 1392-1397, 2003

[35] B-K. Teo, Y. Seo, S. L. Bacharach, J. A. Carrasquillo, S. K. Libutti, H. Shukla, B. H. Hasegawa, R. A. Hawkins, and B. L. Franc, "Partial-volume correction in PET: validation of an iterative postreconstruction method with phantom and patient data," J Nucl Med, 48(5), p. 802-810, 2007

[36] O. Rousset, A. Rahmim, A. Alavi, and H. Zaidi, "Partial volume correction strategies in PET," PET clinics, 2(2), p. 235-249, 2007

[37] M. Soret, S. L. Bacharach, and I. Buvat, "Partial-volume effect in PET tumor imaging," J Nucl Med, 48(6), p. 932-945, 2007

[38] J. E. Mourik, M. Lubberink, U. M. Klumpers, E. F. Comans, A. A. Lammertsma, and R. Boellaard "Partial volume corrected image derived input functions for dynamic PET brain studies: methodology and validation for [11C] flumazenil," Neuroimage, 39(3), p. 1041-1050, 2008

[39] P. Zanotti-Fregonara, E. M. Fadaili, R. Maroy, C. Comtat, A. Souloumiac, S. Jan, M-J. Ribeiro, V. Gaura, A. Bar-Hen, and R. Trébossen, "Comparison of eight methods for the estimation of the image-derived input function in dynamic 18F-FDG PET human brain studies," J Cer Blood Flow Metab 29(11), p. 1825-1835, 2009

[40] J. E. M. Mourik, M. Lubberink, F. H. P. van Velden, R. W. Kloet, B. N. M. van Berckel, A. A. Lammertsma, and R. Boellaard, "In vivo validation of reconstruction-based resolution recovery for human brain studies," J Cereb Blood Flow & Metab, 30(2), p. 381-389, 2010
[41] N. J. Hoetjes, F. H. van Velden, O. S. Hoekstra, C. J. Hoekstra, N. C. Krak, A. A. Lammertsma, and R. Boellaard, "Partial volume correction strategies for quantitative FDG PET in oncology," Eur J Nucl Med Mol Imag, 37(9), p. 1679-1687, 2010
[42] N. A. Karakatsanis and A. Rahmim, "Whole-body PET parametric imaging employing direct 4D nested reconstruction and a generalized non-linear Patlak model," Proc. SPIE Med Imag: Phys Med Imag, 90330Y, 2014
[43] N. A. Karakatsanis, M. A. Lodge, Y. Zhou, M. Casey, R. Wahl, R. Subramaniam, H. Zaidi and A. Rahmim. "Novel multi-parametric SUV/Patlak FDG-PET whole-body imaging framework for routine application to clinical oncology," J Nucl Med, 56 (suppl. 3), p. 625, 2015
[44] Mullani, N. A., Markham, J., & Ter-Pogossian, M. M. (1980). Feasibility of time-of-flight reconstruction in positron emission tomography. J Nucl Med,21(11), 1095-7
[45] M. M. Ter-Pogossian, N. A. Mullani, D. C. Ficke, J. Markham, and D. L. Snyder, "Photon time-of-flight-assisted positron emission tomography," J Comp Assist Tom, 5(2), p. 227-239, 1981
[46] N. A. Mullani, D. C. Ficke, R. Hartz, J. Markham, and G. Wong, "System design of fast PET scanners utilizing time-of-flight," IEEE Trans Nucl Sc, 28(1), p. 104-108, 1981
[47] M. M. Ter-Pogossian, D. C. Ficke, M. Yamamoto, and J. T. Hood Sr, "Super PETT I: a positron emission tomograph utilizing photon time-of-flight information," IEEE Trans Med Imag, 1(3), p. 179-187, 1982
[48] T. K. Lewellen, "Time-of-flight PET," Sem Nucl Med 28(3), p. 268-275, 1998
[49] W. W. Moses, "Time of flight in PET revisited," IEEE Trans Nucl Sc, 50(5), p. 1325-1330, 2003
[50] W. W. Moses, "Recent advances and future advances in time-of-flight PET," Nucl Instr Meth Phys Res Sect A: Accel, Spectrom, Det Assoc Equipm, 580(2), p. 919-924, 2007
[51] M. Conti, "Focus on time-of-flight PET: the benefits of improved time resolution," Eur J Nucl Med Mol Imag, 38(6), p. 1147-1157, 2011
[52] T. Tomitani, "Image reconstruction and noise evaluation in photon time-of-flight assisted positron emission tomography," IEEE Trans Nucl Sc, 28(6), p. 4581-4589, 1981
[53] S. Surti, J. S. Karp, L. M. Popescu, M. E. Daube-Witherspoon, and M. Werner, "Investigation of time-of-flight benefit for fully 3-DPET," IEEE Trans Med Imag, 25(5), 529-538, 2006
[54] A. Mehranian, and H. Zaidi, "Impact of Time-of-Flight PET on Quantification Errors in MR Imaging–Based Attenuation Correction," J Nucl Med, 56(4), p. 635-641, 2015
[55] C. Cloquet, F. C. Sureau, M. Defrise, G. van Simaeys, N. Trotta, and S. Goldman, "Non-Gaussian space-variant resolution modelling for list-mode reconstruction," Phys Med Biol, 55(17), p. 5045-5066, 2010
[56] C. Comtat, F. C. Sureau, M. Sibomana, I. K. Hong, N. Sjöholm, and R. Trebossen, "Image based resolution modeling for the HRRT OSEM reconstructions software," IEEE Nucl Sc Symp Med Imag Conf (NSS/MIC), p. 4120-4123, 2008
[57] A. Rahmim, and J. Tang, "Noise propagation in resolution modeled PET imaging and its impact on detectability," Phys Med Biol, 58(19), p. 6945-6968, 2013
[58] E. Prieto, I. Domínguez-Prado, M. J. García-Velloso, I. Peñuelas, J. A. Richter, and J. M. Martí-Climent, "Impact of time-of-flight and point-spread-function in SUV quantification for oncological PET," Clin Nucl Med,38(2), p. 103-109, 2013
[59] S. Stute, and C. Comtat, "Practical considerations for image-based PSF and blobs reconstruction in PET," Phys Med Biol, 58(11), p. 3849-3870, 2013
[60] S. Ashrafinia, N. Karakatsanis, H. Mohy-ud-Din, and A. Rahmim, "Towards continualized task-based resolution modeling in PET imaging. SPIE Med Imag, p. 903327-903327, 2014
[61] S. Ashrafinia, H. Mohy-ud-Din, N. Karakatsanis, D. Kadrmas and A. Rahmim, "Enhanced quantitative PET imaging utilizing adaptive partial resolution modeling," J Nucl Med, 55 (Supplement 1), p. 371-371, 2014
[62] A. Rahmim, J. Tang, and H. Zaidi, "Four-dimensional (4D) image reconstruction strategies in dynamic PET: beyond conventional independent frame reconstruction," Med Phys, 36(8), p. 3654-3670, 2009
[63] G. Wang and J. Qi, "Direct estimation of kinetic parametric images for dynamic PET," Theranostics, 3(10), p. 802, 2013
[64] W. Zhu, Q. Li, B. Bai, P. S. Conti, and R. M. Leahy, "Patlak image estimation from dual time-point list-mode PET data," IEEE Trans Med Imag 33(4), p. 913-924, 2014
[65] W. Zhu, N. Guo, B. Bai, P. S. Conti, R. M. Leahy, and Q. Li, "Direct estimation from list-mode data for reversible tracers using graphical modeling," IEEE Int Symp Biom Imag (ISBI), p. 1204-1207, 2015
[66] C. S. Patlak and R. G. Blasberg, "Graphical evaluation of blood-to-brain transfer constants from multiple-time uptake data. Generalizations," J. Cereb. Blood Flow Metab., 5, p. 584-590, 1985
[67] N. A. Karakatsanis, Y. Zhou, M. A. Lodge, M. E. Casey, R. L. Wahl, H. Zaidi and A. Rahmim, "Quantitative whole-body parametric PET imaging incorporating a generalized Patlak model," IEEE Nucl Sc Symp Med Imag Conf (NSS/MIC), p. 1-9, 2013
[68] N. A. Karakatsanis, Y. Zhou, M. A. Lodge, M. E. Casey, R. L. Wahl, H. Zaidi and A. Rahmim "Generalized whole-body Patlak parametric imaging for enhanced quantification in clinical PET," Phys Med Biol, 60(22), p. 8643-8673, 2015
[69] J. Yan, B. Planeta-Wilson, and R. E. Carson, "Direct 4-D PET list mode parametric reconstruction with a novel EM algorithm," IEEE Trans Med Imag, 31(12), p. 2213-2223, 2012
[70] K. Lange, D. R. Hunter, and I. Yang, "Optimization transfer using surrogate objective functions," J Comput Graph Stat, 9(1), p. 1-20, 2000
[71] G. Wang, and J. Qi, "Acceleration of the direct reconstruction of linear parametric images using nested algorithms," Phys Med Biol, 55(5), p. 1505-1517, 2010
[72] Y. Zhou, S. Zhang, J. Zhang, N. Karakatsanis, A. Rahmim, M. Lodge, R. Wahl, D. Wong, and R. F. Wang, "Generalized population-based input function estimation given incomplete blood sampling in quantitative dynamic FDG PET studies," J Nucl Med, 53 (Supplement 1), p. 380-380, 2012
[73] N. Karakatsanis, Y. Zhou, M. Lodge, M. Casey, R. Wahl, R. Subramaniam, A. Rahmim, and H. Zaidi, "Clinical Whole-body PET Patlak imaging 60-90min post-injection employing a population-based input function," J Nucl Med 56, (Supplement 3), p. 1786-1786, 2015
[74] G. Akamatsu, K. Ishikawa, K. Mitsumoto, T. Taniguchi, N. Ohya, S. Baba, K. Abe, and M. Sasaki, "Improvement in PET/CT image quality with a combination of point-spread function and time-of-flight in relation to reconstruction parameters," J Nucl Med, 53(11), p. 1716-1722, 2012
[75] N. A. Karakatsanis, M. A. Lodge, M. E. Casey, H. Zaidi and A. Rahmim, "Impact of Acquisition Time-Window on Clinical Whole-Body PET Parametric Imaging," IEEE Nucl Sc Symp Med Imag Conf (NSS/MIC), 2014